Maximum Vortex-Induced Vibrations of a square prism

A. Barrero-Gil[*] and P. Fernandez-Arroyo

Aerospace Thermal and Fluids Mechanics Department, School of Aeronautics, Universidad Politecnica de Madrid, Plaza Cardenal Cisneros 3, 28040, Madrid, Spain

Abstract. This paper presents an experimental investigation concerning the peak amplitudes of oscillation of a square prism due to Vortex-Induced-Vibrations (VIV) as a function of the mass damping parameter $m^*\zeta$ (the so called Griffin--plot); m^* and ζ being, respectively, the non-dimensional mass and the mechanical (structural) damping ratio. With this purpose in mind, an electromagnetic actuator has been employed to provide controlled damping. During the experiments the mass--damping parameter was in the range $0.15 < m^*\zeta < 2.4$. Experiments show that there is a value of $m^*\zeta$ below which VIV appears combined with galloping and the prism oscillation increases monotonically with the incoming flow velocity. For $m^*\zeta > 0.3$ the present experiments show a well-defined VIV phenomenon and, consequently, a Griffin-plot can be defined.

Keywords: Vortex-Induced Vibrations; Griffin plot; square prism

1. Introduction

For more than half a century now, Vortex-Induced-Vibrations (VIV) has been recognized as one of the central problems of the aero/hydro-elasticity field. It is concerned with the interaction between an elastic circular cylinder (or other body with an aerodynamically bluff cross-section) and an incoming flow. Briefly outlined, VIV is due to the periodic shedding of vortices that can excite the body into resonant oscillations when the vortex shedding frequency and body frequency are sufficiently close to one another. Under certain conditions, significant oscillations can emerge (principally, normal to the incident flow). Then, a coupling between the oscillating body and the flow field around it develops with two relevant consequences: (i) there is a range of flow velocities where the vortex shedding frequency is synchronized with the frequency of oscillation (*lock-in* regime), and (ii) the cylinder response may exhibit hysteresis, with jumps in oscillation amplitude and in the fluid forces acting on the body. VIV has much relevance in engineering, with applications to slender chimneys stacks, bridges, tall buildings, offshore structures, electric power lines and heat exchange tubes, among others. Very recently, VIV and other Flow-induced vibration phenomena have also attracted interest as a new way for energy harvesting (Wang and Ko 2010, Sanchez-Sanz *et al.* 2009, Barrero-Gil *et al.* 2010). Because of its practical and scientific relevance, VIV has led to a large number of fundamental studies, many of which are reviewed by Bearman (1984), Sarkpaya (2004), and Williamson and Govardhan (2004), Kaneko *et al.* (2008).

*Corresponding author, Associate Professor, E-mail: antonio.barrero@upm.es

The canonical arrangement for the study of VIV consists of a spring mounted circular cylinder restricted to move in the transverse direction. Such a system can be described by the following structural parameters: cylinder with mass per unit length m, diameter D, length L, a characteristic frequency of oscillation f_N (normally defined in still air), and mechanical damping ratio ζ. The fluid parameters are the velocity of the incoming flow U (turbulence is not considered) and fluid properties ρ (density) and ν (kinematic viscosity). Therefore, taking ρ, D, and f_N as the fundamental physical quantities, the normalized amplitude $A* = A/D$, and frequency of oscillation $f* = f/f_N$ present the following dependence

$$A*, \ f* = \Phi_{1,2}(m*, \zeta, U*, \mathrm{Re}, L/D) \tag{1}$$

where $* = f/f_N$ $m* = m/(\rho D^2)$ is the mass ratio (the dimensionless number typifying the ratio of the mean density of the body to the density of the flow), $U* = U/(f_N D)$ is the reduced velocity, and $\mathrm{Re} = UD/\nu$ is the Reynolds number.

Over the years, extensive research has been conducted for the determination of this relationship (Eq. 1), by means of experimental, theoretical, and computational investigations. Researchers have been concerned principally with the oscillations of an elastically mounted rigid cylinder (for example, see Feng (1968) for $m* \gg 1$ and Khalak and Williamson (1999) for $m* \sim 1$); with the oscillations of long flexible circular cylinders (Brika and Laneville 1993); with forced oscillations of circular cylinders (Bishop 1964, Sarpkaya 1964, Hover *et al.* 1998); with computational studies for low Reynolds number (Evangelinos and Karniadakis 1999, Prasanth and Mittal 2008, Sanchez-Sanz and Velazquez 2009, 2011, Semin *et al.* 2012, Vasallo *et al.* 2012; and with visualization studies of the wake structure (Williamson and Roshko 1988). From the theoretical point of view, some mathematical models based on the wake-oscillator concept of Birkhoff (1957) have been proposed (Gabbai and Benaroya 2005, or Facchinetti *et al.* 2004), as well as the use of potential flow models to describe the fluid forces (Parkinson 1974).

One of the important issues from the structural engineering point of view involves being able to predict the maximum amplitude of oscillations; therefore, determining the peak amplitude of oscillation, A_M^*, as a function of the elastic properties of the cylinder is of great interest. In fact, the Griffin--plot (it will be introduced appropriately later) has become an integral part of the offshore design codes. In this case, $U*$, disappears as a relevant parameter of the problem since we are not interested in the velocity at which A_M^* is achieved. Over the years, the influence of both Re and the aspect ratio *L/D* has not been considered (only Govardham and Williamson (2006), have considered recently their effect). Thus, $A_M^* = \phi_1(m*, \zeta)$ and when $m* \gg 1$ a heuristic argument can be resorted to in order to combine both parameters into a single one, the so called mass-damping parameter $m*\zeta$, leads to the functional relationship $A_M^* = \phi_2(m*\zeta)$, as was showed by Bearman (1984). Let us to summarize his reasoning: a system such us that shown in Fig. 1 has a governing equation of motion given by

$$m(\ddot{y} + 4\pi\zeta \ f_N \dot{y} + 4\pi^2 \ f_N^2 y) = \frac{1}{2}\rho U^2 D C_Y(t) \tag{2}$$

where C_Y is the fluid force coefficient in the transverse direction. In the lock-in region (or resonance range), to a good approximation the fluid force and the cylinder displacement can be described as

$$C_Y(t) = C_{Y0} \sin(2\pi f t + \phi)$$
$$y(t) = A \sin(2\pi f t)$$

(3)

where f is the oscillation frequency and ϕ is the phase angle between the fluid force and the cylinder displacement. Substituting Eq. (3) in Eq. (2) and equating sine and cosine terms, the solution for the response amplitude and frequency is

$$A^* = \frac{C_{Y0} \sin \phi}{16\pi^2 m^* \zeta} \left(\frac{U^{*2}}{f^*} \right)$$

$$f^* = \left(\frac{1 - C_{Y0} \cos \phi U^{*2}}{8\pi^2 m^* A^*} \right)^{1/2}$$
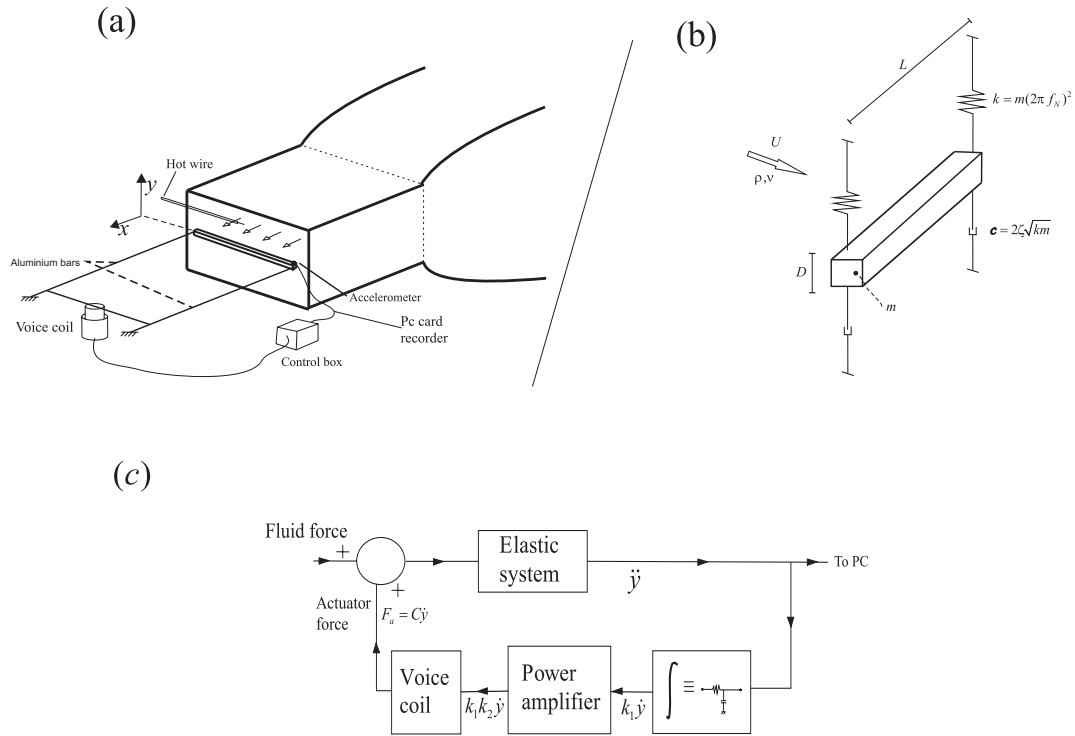
(4)

Fig. 1 Experimental set-up (a) and equivalent mechanical oscillator (b). In (c) an schematic block diagram of the system employed to provide control in damping is sketched.

For large mass ratio, $m* \gg 1$ (a very common situation on structures under wind action), from Eq. (4) one can see that $f* \rightarrow 1 (U*^2 / 8\pi^2 \sim 1$ and experiments show that $C_{Y0} \cos \phi \sim 1)$, and $(U* / f*) \rightarrow St^{-1}$ (herein St is the stationary cylinder Strouhal number). Then, one may deduce that the maximum response amplitude is a function of mass-damping parameter ($m*\zeta$). For $m* \sim 1$, some experiments (see Williamson and Govardhan 2008) have shown that using $m*\zeta$ can be valid as well. The plotting of peak amplitudes versus the mass damping parameter is known as the Griffin--plot, after his first extensive compilation of existing data in the 1970s for the case of circular cylinders.

However, despite its geometrical and practical significance, experimental studies of the VIV response of square prisms are scarce and to date, to the authors' knowledge, there is no Griffin--plot published. The study of the VIV phenomena for square prims in the literature include the experimental measurements of pressure fluctuations acting on an oscillating square prism at amplitudes up to $A* = 0.25$ in the range of reduced velocities of 4-13 by Bearman and Obasaju (1982), hereafter referred to as B--O. The work of Kumar and Gowda (2006), hereafter referred to as K--G, concerns the free vibrations of a spring-mounted square prism, but just for a single value of $m*\zeta = 0.3$ (thanks to our experimental set up, we can study this free vibrations on a large range of $m*\zeta$). The case of an elastic square prism was studied experimentally by Wang and Zhou (2005).

The aim of this study is to characterize experimentally the maximum amplitudes of oscillation for the case of spring-mounted square prisms under VIV. This characterization can be useful for structural designers (we will propose a functional relation between the A_M^* and $m*\zeta$ (also known as Scruton number by wind Engineers), Homma *et al.* (2009)), as well as for scientific purposes. The noticeable difference with respect to the case of a circular cylinder is that for low values of $m*\zeta$ there is an interaction between VIV and transverse galloping, leading to a response that is not self-limited (in the sense that as $U*$ is greater $A*$ increases without limit). In this case, the Griffin--plot has no physical sense.

The mechanism behind galloping is different from that associated with VIV. Basically, galloping is a movement-induced vibration appearing when the velocity of the incident flow exceeds a certain critical value. Then, the stabilizing effect of structural damping is overcome by the destabilizing effect of the fluid force, and a small transverse displacement of the body creates a fluid force in the direction of the motion that tends to increase the amplitude of vibration. The quasi-steady approach predicts the reduced velocity at which galloping appears is $U_g^* = 8\pi m*\zeta / a_1$, where $a_1 = (dC_Y / d\alpha)_{\alpha=0}$ is the slope of C_Y versus the angle of attack measured in static conditions (a more detailed explanation can be found in Parkinson (1974) or Barrero-Gil *et al.* (2009)). Therefore, as $m*\zeta$ diminishes U_g^* is lower and VIV can appear combined with galloping. In the present experiments, VIV phenomenon has appeared well separated from galloping until $m*\zeta \approx 0.3$.

The organization of the paper is as follows: in Section 2 we present the experimental set-up and the method used to actively control the mechanical damping of the system. In Section 3 some experimental results and a Griffin-Plot (the heart of this investigation) are presented. The final section is devoted to summarize several aspects of this investigation.

2. Experimental details

An experimental facility was employed satisfying two major purposes, such as to get linear stiffness, and provide control of mechanical damping. The experimental set--up is similar to that employed by Kumar and Gowda (2006). As it can be seen in Fig. 1(a), a square prism of length L = 30 cm was supported elastically by means of two aluminium beams (40 cm long). The square section prism was made out of wood with smooth surface finishing, and it was subjected to the action of an airstream supplied by a small open-test section wind tunnel of rectangular area of 25 cm height, and 40 cm width. The tunnel consist of a centrifugal fan where the air is powered and sent to the contraction zone (2.4:1 area ratio), and a rectangular duct with two low porosity screens to reduce non--uniformities of the flow up to 1\% in the test section. The speed range of the tunnel is 0.1 to 2.5 m/s. The prism was situated horizontally 6 cm downstream of the exit of the tunnel.

In all cases, the width of the square cross-section D was 2 cm, giving and aspect ratio L/D of 15, and the wind speed U was varied in the range 50-200 cm/s (so that, the Reynolds number, defined as $\text{Re} = UD/\nu$ varied between 1000 and 4000). The free-stream turbulence level at the centerline was below 2%. The transverse vibration, $y(t)$, was obtained with a miniature accelerometer with a resolution of 2 mg (2.5 grams mass and placed at the end of one of the aluminium beams), through double integration of the measured acceleration. This integration was done by using the trapezoidal rule and applying a high pass filter to remove low frequency content. The wind tunnel speed was measured with a portable hot wire anemometer (resolution of 0.01 m/s) placed at $x = -2.5D$ and $y = 4.5D$ (being x the direction of the flow, see Fig. 1(a)). Finally, it should be noted that the experimental set-up allows for a small motion in the x direction (typically, $x/y < 0.01$).

2.1 Control of mechanical damping

To provide accurate control of damping, a voice coil was used as an actuator. The voice coil produces a force that is proportional to the current drive through the coil. If $V_a(t)$ is the voltage across the coil, R its electrical resistance and $z(t)$ the displacement of the coil, then the force F_a supplied by the voice coil is given approximately by (the coil inductance and capacitance can be neglected)

$$F_a(t) = \frac{K}{R}V_a(t) - \left(\frac{K^2}{R} + b\right)\dot{z} \tag{5}$$

where K is a constant and b another constant which takes into account the eddy current effects. If $V_a(t)$ is proportional to the transverse velocity of vibration $\dot{y}(t)$, and $z(t)$ is proportional to the transverse vibration amplitude of the square prism, then

$$F_a(t) = C\dot{y}(t) \tag{6}$$

where C is a constant. Therefore the voice coil introduces an external damping term in the system dynamics, which now can be written as

$$m(\ddot{y} + 4\pi\zeta_0\dot{y} + 4\pi^2 f_N^2 y) = \frac{1}{2}\rho U^2 DC_Y(t) + F_a(t) = \frac{1}{2}\rho U^2 DC_Y(t) + C\dot{y} \tag{7}$$

where m is the equivalent mass of the system (mass of the square prism plus the modal mass of the beam system) per unit length and ζ_0 is the mechanical damping without control. To calculate the equivalent mass, firstly the stiffness of the installation was measured by adding calibrated weights to the center of the square prism and measuring its vertical displacement with a vernier caliper. The square prism was then excited with an initial displacement giving a natural frequency of oscillations of $f_N = 5.3$ Hz. The equivalent mass is then deduced as $m = k/(2\pi f_N^2)$. A value of $m = 0.176$ kg/m was obtained ($m^* = 353$).

As it can be seen in the block diagram shown in Fig. 1(c), the output voltage of the accelerometer V_{acc} (proportional to $\ddot{y}$) is integrated by means of a passive low--pass filter with cut-off frequency of 0.15 Hz (as the natural frequency of the system was 5.3 Hz the phase lag introduced is less than 2°), so that $V_2(t) = \frac{1}{R_F C_F}\int V_{acc}(t)dt = k_1\dot{y}(t)$ (R_F and C_F are, respectively, the resistance and capacitance of the low--pass filter; k_1 is a constant]. Then, V_2 is sent to the power amplifier that drives the voice coil with a voltage proportional to the velocity of oscillation, $V_a(t) = k_1 k_2\dot{y}(t)$ (and hence $F_a = C\dot{y}$). The magnitude of the damping introduced, C, is varied with a potentiometer and its sign can be changed if the polarity of V_a is reversed, providing accurate control of positive and negative damping. At the same time, the accelerometer signal is recorded on a PC using a 12 bit A/D board at a sampling frequency of 200 Hz. Finally, it should be noted that the voice coil is placed downstream of the square prism far enough so that $z << y$ and the voice coil has a linear behavior.

2.2 Experimental procedure

All experiments begin with a characterization of mechanical properties without incoming flow (in still air). As active control is only used in damping, for all cases the measured frequency of oscillation was nearly the same (5.3 Hz). Damping in still air can be divided in two components: damping caused by fluid viscosity and mechanical damping caused by internal friction. The fluid viscosity damping force F_{hd} per unit length can be estimated introducing a non-dimensional drag coefficient C_d

$$F_{hd} = -\frac{1}{2}\rho C_d |\dot{y}|\dot{y} \tag{8}$$

Assuming sinusoidal motion with amplitude A and frequency f, and taking only the first term of the Fourier expansion of Eq. (8) (Blevins 1990)

$$F_{hd} = \frac{8}{3}\rho C_d AfD\dot{y} \tag{9}$$

On the other hand, the mechanical damping force per unit length, F_{md}, is given by

$$F_{md} = 4\pi \; fm\zeta \; \dot{y} \tag{10}$$

so that

$$\frac{F_{md}}{F_{hd}} = \frac{3\pi m * \zeta}{2C_d A *} \tag{11}$$

It follows that $F_{md} / F_{hd} \sim 1$ for low values of $m*\zeta$ and the total damping, mechanical (ζ) plus hydrodynamic (ζ_h), has a highly non-lineal dependence on the amplitude of oscillations. Experiments (see for example Brika and Laneville (1993)) show that ζ_h can be approximated by a quadratic dependence on the amplitude of the oscillations (C_d is dependent on amplitude of the oscillation), and therefore the mechanical damping can be estimated by simply subtracting the hydrodynamic component from the measured (total) damping (ζ_{sa}). That is, $\zeta = \zeta_{sa} - k(A/D)^2$, where k is positive and constant. One can see then that the mechanical damping can be evaluated measuring the damping in still air ζ_{sa} and extrapolating its value as A/D tends to zero. Here, the total damping is determined by measuring the decay between two consecutive peak amplitudes,

$$\zeta_{sa}(A_i) = \frac{1}{2\pi} \ln \frac{A_i}{A_{i+1}} \tag{12}$$

Fig. 2 shows two free-decay tests used to obtain damping characteristics as a function of the amplitude of oscillations. Cases (a) and (b) correspond, respectively, to the case when the damping introduced by the actuator is negative (ζ =0.00146) and positive (ζ =0.0047), since the damping without actuation is ζ_0 =0.0029.
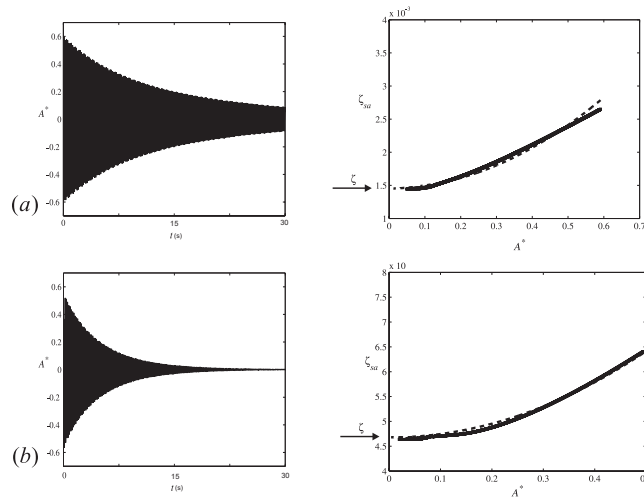

Fig. 2 Positive [case (b)] and negative [case (a)] damping introduced in the system. In both cases the trace of the displacements recorded is shown (left) as well as the total damping as a function of the normalized amplitude of oscillations (right). Dashed line corresponds to a square law fitting of experimental measurements

3. Results

After the mechanical damping was imposed and measured, the experimental procedure was always the same: fixing the airstream velocity, the square prism is exposed over sufficiently long time until a steady state of oscillation is reached; then, the oscillation is registered during 60 seconds. Next, the flow velocity is increased in a small step with the prism still oscillating and the operation is repeated. During the experiments, no hysteresis effects were observed, and when the flow velocity was decreased the results were very nearly the same. In fact, when the model was released from rest, the steady amplitude of oscillation $A*$ was approximately the same than when the model was released from a high amplitude (Fig. 3).
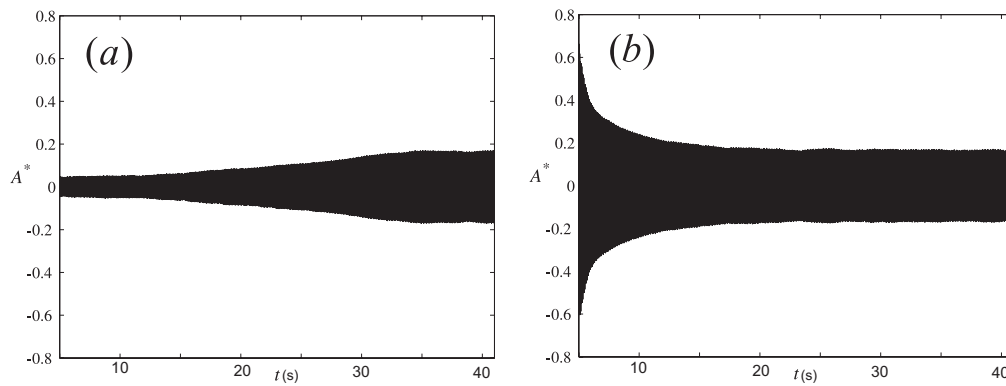

Fig. 3 Traces of the vibration amplitude for $U* = 11.8$ with two different initial conditions: (a) from rest, (b) with pre-excitation

Looking at the figure it is observed that the time needed to reach the steady state depends on the initial condition, being much lower when there is pre-excitation (in fact, we have observed that the decay rate is even larger than that of still air conditions, indicating a strong energy transfer from the body to the flow). The absence of hysteresis matches with the experimental visualization studies carried out by Ongoren and Rockwell (1988), as well as the experimental results of K--G. For the square cross-section oscillating at a fixed amplitude ($A* = 0.13$), Ongoren and Rockwell did not detect a phase change of the vortex shedding relative to the body motion when $f / f_v \sim 1$ (f and f_v are, respectively, the frequency of oscillation and the frequency of vortex shedding); however, they observed an abrupt discontinuity for the case of a circular cylinder, which could be responsible for the hysteresis phenomenon.

Experimental results of K--G are shown in Fig. 4 together with results of the present investigation. The overall shape and the range of lock-in is similar in both experiments (comparable to that observed by B--O), but several differences are noted. The most remarkable findings is that the reduced velocities at which the maximum amplitudes are reached are different. A value of $U* = 10$ is found in the K--G results and $U* = 12.5$ in our results. However, quantitative comparison is not easy, due to the different experimental conditions. The Reynolds number in the K--G experiments was in the range $4000 \leq \mathrm{Re} \leq 14000$ (our experiments are in the range $1000 \leq \mathrm{Re} \leq 4000$ 1000), and the aspect ratio was also different ($L/D = 11.6$ in K--G, and
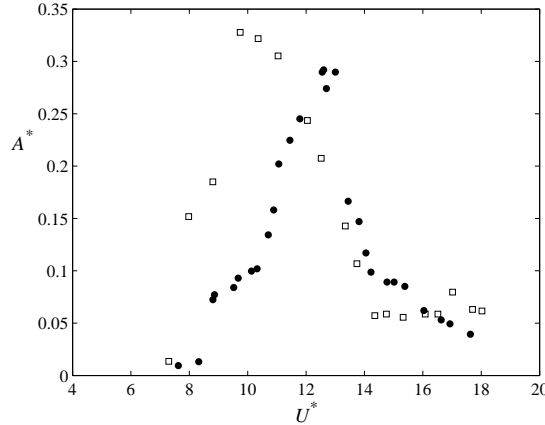
L/D in our experiments).

Fig. 4 Amplitude response A^* versus reduced velocity U^*. White squares: K--W results ($m^* \zeta = 0.3$). Present investigation in black circles ($m^* \zeta = 0.45$)

Fig. 5 shows the non-dimensional amplitude, A^* as a function of the reduced velocity U^* for three different damping ratios ($m^* \zeta$ =0.68, 0.62, 0.45). Note that oscillations start at $U^* \approx 7.5$. This value corresponds to a Strouhal number of 0.13, which is close to some experimental measurements (Okajima 1982). Then, A^* increases until $U^* \sim 12-13$, where a drastic reduction in A^* takes place. Finally, the amplitude of oscillations monotonically decreases with flow velocity in the range $U^* \sim 14-17$. As expected, both the maximum amplitude during lock-in and its extent are inversely proportional to $m^* \zeta$.

Measurements of the fluctuating lift force were not attempted in the present experiments. However, Parkinson (1974), estimated the lift coefficient in phase with the square prism velocity ($C_{Y0} \sin \phi$) from Eq. (4). That is

$$C_{Y0} \sin \phi = 16\pi^2 m^* \zeta \left(\frac{f^* A^*}{U^{*2}} \right) \tag{13}$$

Results are shown in Fig. 6 for two values of the mass damping parameter. It is remarkable that the maximum value of $C_{Y0} \sin \phi$ appears at $U^* = 12$ in both cases. Measurements of the phase angle between suction, measured at the centre of a side face, and square prism displacement carried out by B--O show a maximum value for $\sin \phi$ at $U^* = 12$ when $A^* = 0.25$ (Fig. 14 in B--O paper). It is precisely the reduced velocity at which our free vibration results present a peak. B--O states that maximum amplitudes could occur at the high velocity end of lock-in. Our results are in good agreement with this observation (however, it must be noted that forced oscillations with a given amplitude and frequency do not represent completely the case of a free vibration arrangement, where amplitude and frequency are changing).

During the experiments we found that there is a certain value of the mass--damping parameter at which the character of response is very different, due to the effects of galloping. As can be seen

in Fig. 7, for very low values of damping, the oscillations start where the stationary Strouhal number predicts ($U* \approx 7.5.$), but $A*$ always increases with $U*$ without apparent limit (our wind tunnel has a maximum flow velocity of some 2 m/s). For these cases, the Griffin--plot is not defined.
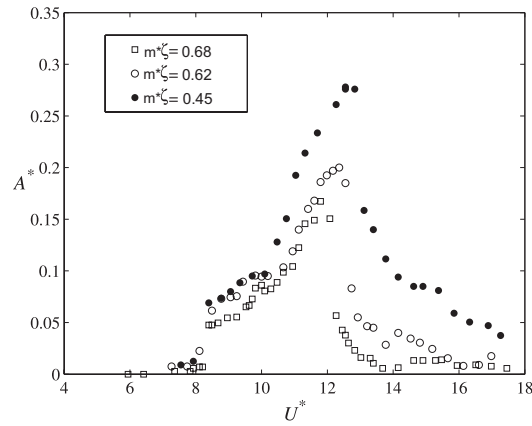

Fig. 5 Amplitude response A^* versus reduced velocity U^* for three damping levels
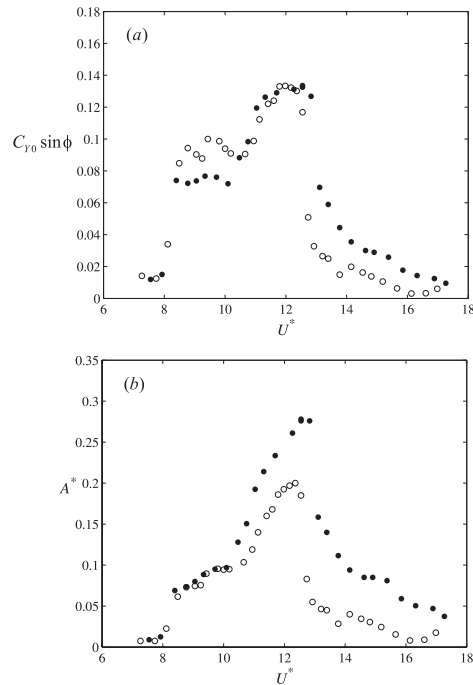

Fig. 6 Fluid excitation (a) [based on Eq. (4)] and square prism response (b) for two values of damping. White circles: $m*\zeta = 0.62$. Black circles: $m*\zeta = 0.45$
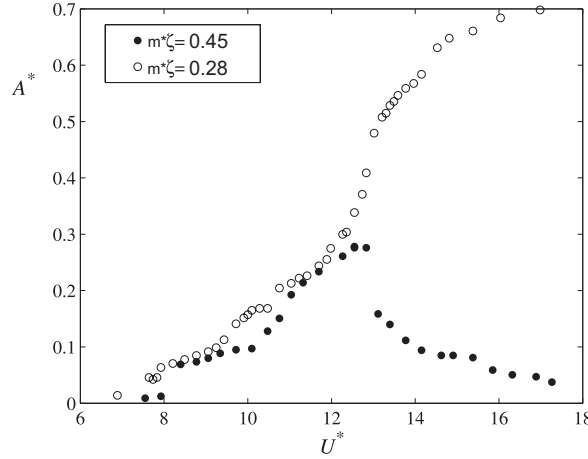
Fig. 7 Square cylinder response A^* versus the reduced velocity U^*. For very low values of the mass damping parameter VIV appears combined with galloping

We did not observe oscillations below $U^* = 7.5$ (a case with $m^*\zeta$ as low as 0.15 was tested). This result is consistent with the phase measurements of B--O, where the phase angle ϕ is negative below $U^* = 7.8$ when $A^* = 0.05$ (and hence there is no energy transfer between the flow and the square prism, see Eq. (4)).

We conducted 30 tests similar to those showed in Fig. 5 covering the range $0.15 \leq m^*\zeta < 2.4$ looking for the Griffin--plot, i.e the functional relationship between A_M^* and $m^*\zeta$. The results are plotted in Fig. 8. A least-square fitting to the data gives the following dependence

$$A_M^* = 0.47 - 1.1d^* + 0.91d^{*2} - 0.24d^{*3} \tag{14}$$

where a convenient variable $d^* = m^*\zeta - 0.3$ (valid for $m^*\zeta > 0.3$) has been introduced (note that the present experiments show than for $m^*\zeta < 0.3$ galloping appears and the response is not self-limited). For completeness, the figure also shows experimental data from other researchers.

The extension of the range of resonance (lock-in) is plotted in Fig. 9. Here, we have defined the lock-in by an oscillation amplitude threshold, namely $A^*(U^*) > 0.05$. As it can be seen, the lock-in domain increases as d^* tends to zero. Very different is the behavior of the upper limit, U_U^*, compared to that of the lower limit U_L^*. While U_L^* remains almost independent of d^*, U_U^* shows an increasing derivative as d^* diminishes. A possible explanation can be given here: U_L^* is mainly governed by the vortex shedding frequency when the square section is almost at rest, and therefore, it should be almost independent of the mechanical properties m^* and ζ. A least-square fitting gives the following dependence

$$U_L^* = 7.9 + 0.28d^*, \quad U_U^* = 10(1 - e^{-2.1d^*}) \tag{15}$$
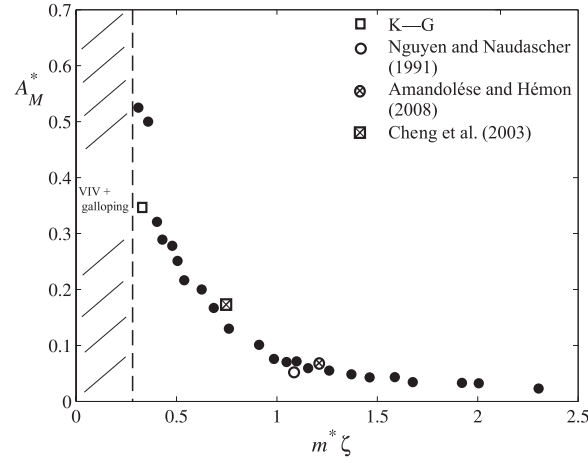
A. Barrero-Gil and P. Fernandez-Arroyo

Fig. 8 Griffin--plot: peak amplitudes of oscillation, A^*_M, as a function of the mass--damping parameter for the square cylinder (black circles corresponds to results of the present study). Symbols (excluding black circles) stand for experimental measurements by other researchers [Kumar and Gowda (2006); Nguyen and Naudascher (1991); Amandolèse and Hemon (2010); Cheng et al. (2003)]
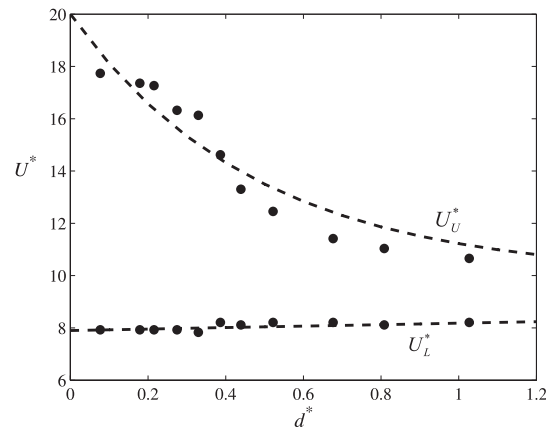

Fig. 9 Lock-in (range of resonance) domain as a function of the damping value ($d^* = m^* \zeta - 0.3$)

4. Conclusions

Most of the experimental studies into VIV have been involved with circular cylinders oscillating in cross-flow, and comparatively few literature is devoted to the case of square prisms.

Here, an experimental apparatus has served as a key tool to study the free vibration due to VIV of a spring-mounted square prism. This allows to vary the mechanical damping without changing the others parameters in the problem (conditions of the incident flow, mass ratio or the aspect ratio). Then, the effect of the mass damping parameter has been studied in detail, and the measured

peak amplitude of vibration presents the following dependence: $A_M^* = 0.47 - 1.1d* + 0.91d*^2 - 0.24d*^3$, where $d* = m*\zeta - 0.3$ is a convenient variable introduced to exclude the range of values where galloping appears combined with VIV ($m*\zeta < 0.3$). With respect to the range of resonance (lock-in), experiments show a behavior similar to that of the circular cylinder. The lower limit, defined as the initial reduced velocity at which oscillations are of significance is almost independent of the mass damping parameter.

However, the upper limit (end of lock-in) increases as the mass damping parameter diminishes, being the lock-in extension inversely proportional to the mass damping parameter.

During the experiments the hysteresis phenomenon typically observed for circular cylinders did not take place. Several tests were carried out with different initial conditions and, whatever the initial condition (square prism at rest or at a high amplitude), the final response was always the same. This fact is consistent with previous experiments and visualization studies.

Finally, it should be noted that here we have studied principally the influence of the mass damping--parameter in the peak amplitudes during VIV. However secondary parameters were present in the experiments, like the turbulence characteristics of the incoming flow. Turbulence can also play an important role in VIV. It is reasonable to think that turbulence disturb vortex shedding reducing the lift and drag fluctuations and, therefore, the amplitude of oscillations. However, this is a very complex open question that needs further study. Also the square prism was mounted with no end plates and, in spite of its relatively high aspect ratio ($L/D = 15$), it is expected that three dimensional effects could have an influence.

References

Amandolese, X. and Hemon, P. (2009), "Vortex-induced vibration of a square cylinder in wind tunnel". www.ladhyx.polytechnique.fr/people/pascal/.../CRASjuillet09.pdf.

Barrero-Gil, A., Sanz-Andres, A. and Alonso, G. (2009), "Hysteresis in transverse galloping: The role of the inflection points", *J. Fluid. Struct.*, **25**, 1007-1020.

Barrero-Gil, A., Sanz-Andres, A. and Alonso, G. (2010), "Energy harvesting from transverse galloping", *J. Sound Vib.*, **329**(14), 2873-2883.

Bearman, P.W. (1984), "Vortex shedding from oscillating bluff bodies", *Ann. Rev.Fluid Mech.*, **16**, 195-222.

Bearman, P.W and Obasaju E.D. (1982), "An experimental study of pressure fluctuations on fixed and oscillating square-section cylinders", *J. Fluid. Mech.*, **119**, 297-321.

Birkhoff ,G. and Zarantello, E.H. (1957), *Jets, wakes and cavities*, Academic press, New York.

Bishop, R.E. and Hassan, A.Y. (1964), "The lift and drag forces on a circular cylinder oscillating in a flowing fluid", *Proceedings Royal Society of London*, Series A, **277**, 51-75.

Brika, D. and Laneville, A. (1993), "The vortex induced vibrations of long flexible circular cylinder", *J. Fluid. Mech.*, **250**, 481-508.

Blevins, R.D. (1990), *Flow-Induced Vibrations*, Krieger publishing company, New York.

Cheng, L. Zhou, Y. and Zhang, M.M. (2003), "Perturbed interaction between vortex shedding and induced vibration", *J. Fluid. Struct.*, **17**, 887-901.

Evangelinos, C. and Karniadakis, G. (1999), "Dynamics and flow structures in the turbulent wake of a rigid and flexible cylinders subject to vortex-induced vibrations", *J. Fluid. Mech.*, **400**, 91-124.

Facchinetti, M.L., de Langre, E. and Biolley, F. (2004), "Coupling of structure and wake oscillators in vortex-induced vibrations", *J. Fluid. Struct.*, **19**(2), 123-140.

Feng, C.C. (1968), *The measurement of vortex induced induced effects in flow past a stationary and oscillating circular and D-section cylinder*, M.A.Sc. Thesis, University of British columbia, Canada.

Gabbai, R.D. and Benaroya, H. (2005), "An overview of vortex-induced vibration of circular cylinders", *J.*

Sound Vib., **282**, 575-616.

Homma, S., Maeda, J. and Hanada, N. (2009), "The damping efficiency of vortex-induced vibration by tuned-mass damper of a tower-supported steel stack", *Wind Struct.*, **12**(4), 333-347.

Hover, F.S., Techet, A.H. and Triantafyllou, M.S. (1998), "Forces on oscillating uniform and tapered cylinders in cross-flow", *J. Fluid. Mech.*, **363**, 97-114.

Govardhan, R. and Williamson, C.H. (2006), "Defining the 'modified Griffin plot' in vortex-induced vibration: revealing the effect of Reynolds number using controlled damping", *J. Fluid. Mech.*, **561**, 147-180.

Kaneko, S., Nakamura, T., Inada, F. and Kato, F. (2008), *Flow Induced Vibrations: Classifications and Lessons from Practical Experiences*, Elsevier Science, 1 Edition.

Khalak, A. and Williamson, C.H. (1999), "Dynamics of a hydroelastic cylinder with very low mass and damping", *J. Fluid. Struct.*, **13**, 813-851.

Kumar, R.A. and Gowda, B.H.L. (2006), "Flow-induced vibration of a square cylinder without and with interference", *J. Fluid. Struct.*, **22**, 345-369.

Nguyen, D.T. and Naudascher, E. (1991), "Vibrations of beams and trashracks in parallel and inclined flows", *J. Hydraul. Eng.- ASCE*, **17**(8), 1056.

Ongoren, A. and Rockwell, D. (1988), "Flow structure from an oscillating cylinder. Part 1. Mechanisms of phase shift and recovery in the near wake", *J. Fluid. Mech.*, **191**, 197-223.

Okajima, A. (1982), "Strouhal numbers of rectangular cylinders", *J. Fluid. Mech.*, **123**, 379-398.

Parkinson, G.V. (1974), *Mathematical Models of Flow-Induced-Vibrations*, Flow-Induced Structural Vibrations, Springer.

Prasanth, T.K. and Mittal, S. (2008), "Vortex-induced vibrations of a circular cylinder at low Reynolds numbers", *J. Fluid. Mech.*, **594**, 463-491.

Sanchez-Sanz, M., Fernández, B. and Velázquez, A. (2009), "Energy harvesting micro-resonator based on the forces generated by the Karman Street around a rectangular cylinder", *J. Microelectromech. Syst.*, **18**(2), 449-457.

Sanchez-Sanz, M. and Velazquez, A. (2009), "Vortex-induced vibration of a prism in internal flow", *J. Fluid. Mech.*, **641**, 431-440.

Sanchez-Sanz, M. and Velazquez, A. (2011), "Passive control of vortex induced vibration in internal flow using body shape ", *J. Fluid. Struct.*, **27**(7), 976-985.

Sarpkaya, T. (2004), "A critical review of the intrinsic nature of vortex-induced vibrations", *J. Fluid. Struct.*, **19**, 389-447.

Sarpkaya, T. (1978), "Fluid forces on oscillating cylinders", *J. Waterw. Port C. –* ASCE, **104**, 275-290.

Semin, B., Decoene, A., Hulin, J.P., François, M.L.M. and Auradou, H. (2012), "New oscillatory instability of a confined cylinder in a flow below the vortex shedding threshold", *J. Fluid. Mech.*, **690**, 345-365.

Vasallo, A., Lorenzana, A and Roosi, R. (2012), "Lock-in and drag amplification effects in slender line-like structures through CFD" , *Wind Struct.*, **15** (3), 189-208.

Wang, Z.J. and Zhou, Y. (2005), "Vortex-induced vibration characteristics of an elastic square cylinder on fixed supports", *J. Fluid. Eng.*, **127**, 241-249.

Wang, D.A. and Ko, H.H. (2010), "Piezoelectric energy harvesting from flow-induced vibration", *J. Micromech. Microeng.*, 20 025019 doi:10.1088/09601317/20/2/025019.

Williamson, C.H. and Govardhan, R. (2004), "Vortex-induced vibrations", *Ann. Rev. Fluid Mech.,* **36**, 413-455.

Williamson, C.H. and Govardhan, R. (2008), "A brief review of recent results in vortex-induced vibrations", *J. Wind Eng. Ind. Aerod.*, **96** (6-7), 13-735.

Williamson, C.H. and Roshko, A. (1988), "Vortex formation in the wake of an oscillating cylinder", *J. Fluid. Struct.*, **2**, 355-381.

CC